

Thermo-exergo-economic analysis of double slope solar still augmented with ferrite ring magnets and GI sheet

Manoj Dubey, Dhananjay R. Mishra*

Department of Mechanical Engineering, Jaypee University of Engineering and Technology, A.B. Road, Guna-47322, Madhya Pradesh, India, Tel. +91-7544-267051/267310-314; emails: dm30680@gmail.com (D.R. Mishra) mpdubey1963@gmail.com (M. Dubey)

Received 3 October 2019; Accepted 3 April 2020

ABSTRACT

Rapid growth in population is enhancing the requirement of the huge amount of potable water at an affordable price. The paper consists of a comparative economic study based on numerical and experimental analysis. The effect of magnetization has been presented on the performance of double slope solar still (2 m × 1 m basin area), longitudinally oriented in an east-west direction, with 15° top cover inclination. Permanent ferrite ring magnets were evenly distributed in the basin water and a blackened galvanized iron sheet is placed over them for uniform distribution of the magnetic field. An identical still, without this arrangement is also run for comparison. Experiments have been carried out at the geographical condition of Jaypee University of Engineering and Technology, Guna (latitude: 24.4348°N, longitude: 77.1606°E, India). Theoretical evaluation of the experimental result has been carried out with the help of the Kumar and Tiwari model. An increase of, 171.83% in the rate of heat transfer, 57.58% in exergy efficiency, 31.13% in distillate yield, 21.77% in evaporative heat transfer coefficient, 16.26% in total heat transfer coefficient, and 22.64% in experimental efficiency is seen. Payback period analysis is also done. It inferred that magnetization improves the performance of the still considerably.

Keywords: Double slope solar still; Solar distillation; Magnetization; Exergy efficiency; Exergy destruction

1. Introduction

The increasing population is continuously emphasizing the increased demand for fresh potable water. A large amount of water is available in a contaminated form that needs recycling/purification. The need of the time is to search for methods to obtain fresh water from the contaminated one. Solar distillation is emerging as a feasible solution to this problem [1]. Solar energy is free of cost, renewable, non-polluting, and abundantly available on the earth's surface. Solar still is a simple device that works on the fundamental principle of evaporation, condensation phenomenon and requires the least maintenance. Researchers are continuously striving for increasing productivity of distiller units by doing various moderations in conventional design to make it more competitive.

Arunkumar et al. [2] have reviewed productivity, modifications, and heat and mass transfer processes occurred in various solar distiller units. The effects of the augmentation of fins, black granite, wick, and external reflectors have been reported by Gnanaraj and Velmurugan [3]. Double slope solar stills of different glass cover inclinations have been tested by Dubey and Mishra [4]. It has been reported that the still with 15° cover inclination performs better than still having 30° or 45° inclination. Holysz et al. [5] have reported that the magnetic field changes the conductivity of electrolyte solutions and water evaporated from it by changing a hydrating water structure around the ion. The effect of the position of the sample of water in the magnetic field regarding evaporation has been reported by Guo et al. [6]. Wang et al. [7] have reported that magnetic field treatment increases evaporation amount, decreases specific heat and lowers

* Corresponding author.

the boiling point of tap water. A decrease in surface tension, an increase in the volume of water evaporated and an increase in productivity of crops by application of magnetic field has been reported by Amor et al. [8]. Cai et al. [9] have studied the effect of the magnetic field on purified water while flowing. They have reported the decrease in surface tension and increase in viscosity of the flowing water, with an increase in effective treatment time. Effect on water evaporation through the magnetic field of 0.5 T, located at different locations of tested water height (water-air interface, water mid-height and bottom) has been reported by Rashid et al. [10]. It has been reported that the preferred location of a magnetic field is a water-air interface where the evaporation rate is increased by 6%, whereas no effect of the magnetic field is observed when applied at the bottom of the water height. Chang and Weng [11] have reported that the number of hydrogen bonds increases slightly as the strength of the magnetic field is increased. This implies that the application of an external magnetic field can also control the size of a water cluster. Nakagawa et al. [12] have proclaimed that the water vaporization rate is significantly influenced by static magnetic fields up to 8T in air and oxygen. The magnitude of the effect depended on the product of field and field-gradient. Seyfi et al. [13] have studied the evaporation rate of deionized water in presence of one, two or three permanent ferrite magnets in two different orientations of the magnetic field (tangential and perpendicular to the air-water interface). They have reported that when the magnetic field is perpendicular to the air-water interface, the evaporation increased by 18.3%. They observed that if the magnetic field was applied perpendicular to the air-water interface for 60 min then the evaporation rate remains higher up to 40 min even after removal of a magnetic field. It has been reported by Szcześ et al. [14] that the magnetic field decreases the water conductivity, which is inversely proportional to the flow rate, and increases the amount of evaporated water, even after the water's distillation. The effects are due to the hydrogen bond network strengthening and the perturbation of gas/liquid interface from the air nanobubbles in the water. Scaling is a problem in solar stills that require removal through a physical and chemical treatment to maintain the efficiency of the system.

The application of a magnetic field is a better way to handle such a problem. It has been reviewed by Zaidi et al. [15] that magnetic field application has the potential to improve the physical performance in terms of solid-liquid separation mainly through the aggregation of colloidal particles. It has been reported by Dumka et al. [16] that the overall internal efficiency and exergy efficiency of single slope solar still are enhanced by the magnetization of water. They have also reported a reduction in exergy destruction in basin water of the still. So far the effect of the magnetic field on evaporation rate thermal conductivity and descaling has been studied in single slope solar stills.

In the present work, a comparative study is done to analyze the effect of a uniform permanent magnetic field on coefficients of heat transfer, thermal efficiency, and exergy efficiency during solar distillation. The experiment is conducted in a single basin double slope-solar-still.

2. Experimental setup

Two identical single basin double slope solar stills have been fabricated using 5 mm thick fiber reinforced plastic and 15° inclined top covers. Top covers were made with 4 mm thick toughened iron glass. Basins of the stills are rectangular (2 m × 1 m). 10 cm elevation is kept at the ends of the walls. Both the stills are made airtight using clay putty to prevent leakage of water vapors from the distiller units. Distillate collection channels are provided on the inner walls. The slope is provided in all the channels to collect the distillate yield at two ends of the solar still. The still without magnets is called conventional double slope solar still (CDSSS). In modified double slope solar still (MDSSS), a rectangular galvanized iron sheet (1.8 m × 0.9 m) painted with dull black color, is dipped horizontally in the basin water, keeping the uniform distance from walls of the still. Thirty-two ferrite ring magnets, each having a magnetic field strength of 90 mT, are placed beneath the GI sheet in uniform array in order to maintain a uniform magnetic field within the basin as shown in Fig. 3. A constant depth of 2.5 cm water was maintained in both the stills. The schematic view of CDSSS and MDSSS are shown in Figs. 1 and 2, respectively. Arrangement of ferrite ring magnets beneath GI sheet

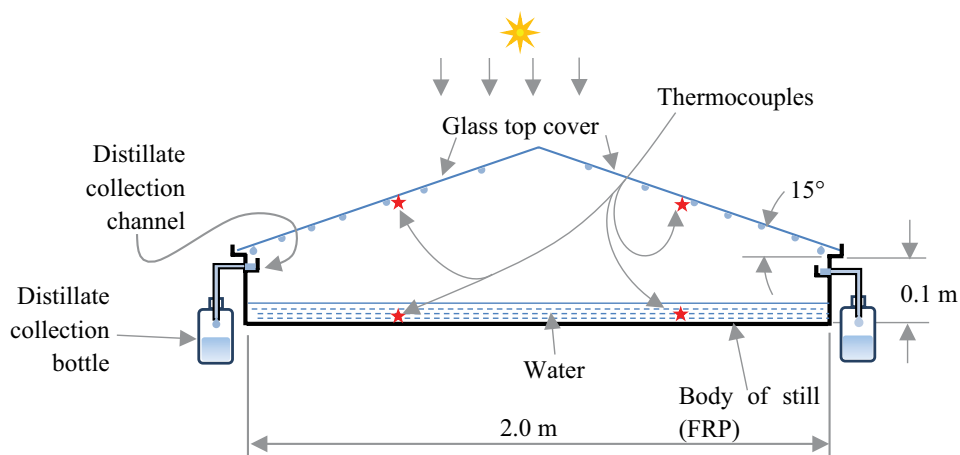


Fig. 1. Schematic representation of CDSSS.

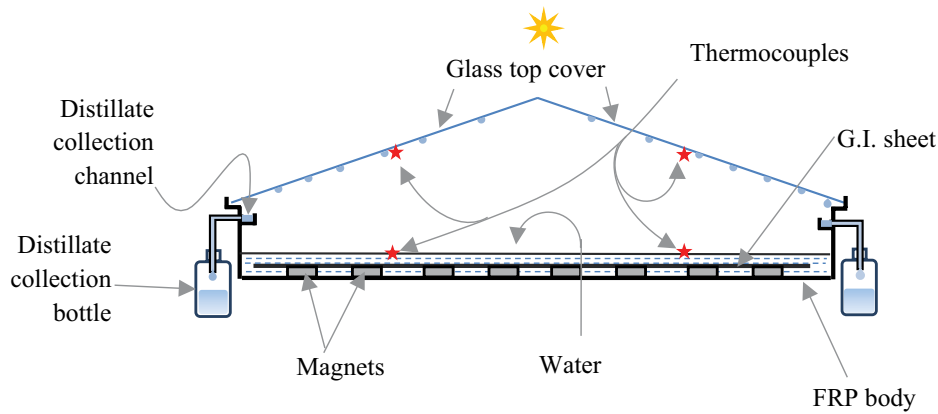


Fig. 2. Schematic representation of MDSSS.

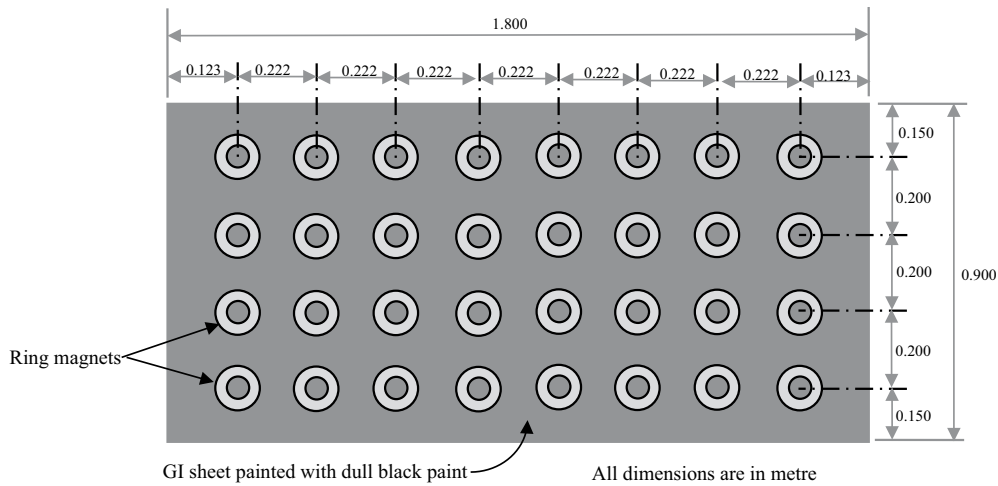


Fig. 3. Schematic view of an arrangement of ferrite ring magnets under black painted GI sheet.

painted with black color, dimensions of ferrite ring magnets and its actual photograph, are shown in Figs. 3, 4a and b, respectively. Fig. 5 shows the photograph of the experimental setup.

During the experimentation, nine K-type thermocouples (K 7/32-2C-TEF) along with temperature indicator DTC324A-2 have been used in MDSSS and CDSSS to measure temperatures of entities such as ambient air, basin water, and an inner surface of condensing glass cover. Incident solar radiation on inclined glass cover surfaces was measured with the help of solar power meter TM-207. Graduated measuring cylinders of 100, 250, 500, and 1,000 ml were used to measure distillate yield obtained from CDSSS and MDSSS.

The enhancement of temperature and rate of surface evaporation will take place due to the incident solar radiation. The mixture of air and water vapors move from the top surface of the water to the inner surface of the condensing glass cover by natural convection where nucleation and droplet formation took place. Due to the presence of cover inclination and gravitation force, it will get collected in the channels and finally gets collected through rubber pipe in bottles placed outside the solar still.

3. Mathematical background

Solar distiller units operate on the fundamental principle of evaporation, condensation, convection, and radiation. The convective heat transfer rate from water to condensing glass cover can be calculated using the following relation [17]:

$$\dot{q}_{c,w-g} = h_{c,w-g} \cdot (T_w - T_g) \tag{1}$$

Dimensionless numbers viz. Nusselt number (Nu), Grashof number (Gr), Prandtl number (Pr) and Rayleigh number (Ra), required for estimating convective heat transfer in solar still one can get [17]:

$$Nu = \frac{h_{c,w-g}}{\left(\frac{k}{d}\right)} = C (Gr \cdot Pr)^n \tag{2}$$

$$Gr = \frac{g \cdot \beta \cdot d^3 \cdot \rho \cdot \Delta T'}{\mu^2} \tag{3}$$

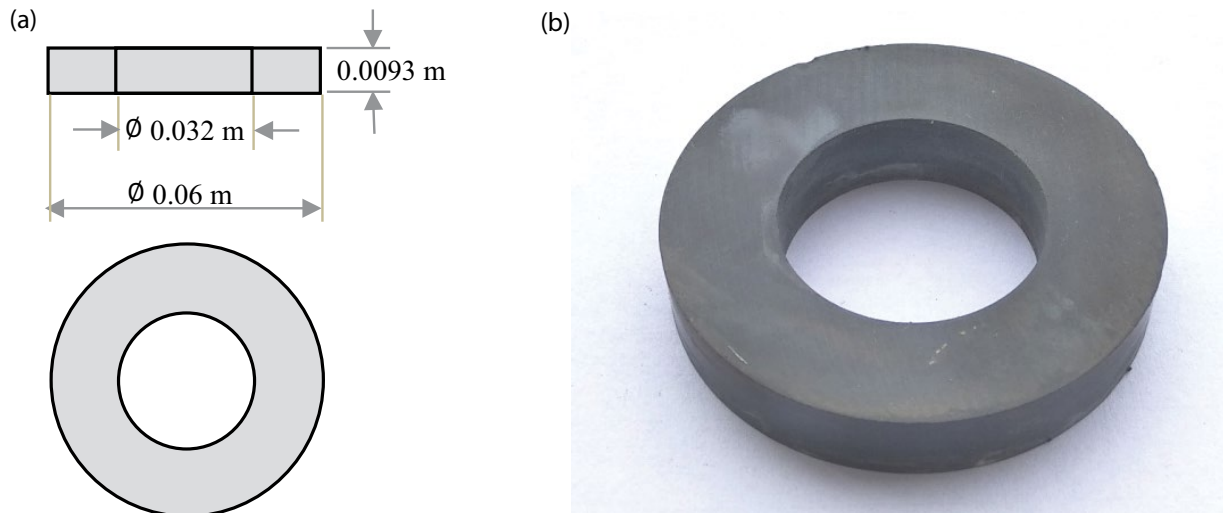


Fig. 4. (a) Dimensions of a ring magnet and (b) photograph of ferrite ring magnet (permanent) used in MDSSS.



Fig. 5. Photograph of the experimental setup of CDSSS and MDSSS.

The effective temperature difference can be calculated using the relation:

$$\Delta T' = T_w - T_g + \frac{(P_w - P_g)(T_w + 273)}{(2.689 \times 10^5 - P_w)} \quad (4)$$

$$\text{Pr} = \frac{\mu \cdot c_p}{k} \quad (5)$$

$$\text{Ra} = \text{Gr} \cdot \text{Pr} \quad (6)$$

For the evaluation of these numbers, the physical properties of the air-water vapor mixture also need to be calculated. These are calculated using empirical relations given by Toyama et al. [18]. For evaluation of $h_{c,w-g}$, values of C and n also be ascertained. Many theoretical models have been proposed by researchers [19,20] for calculating the

values of C and n . Dumka and Mishra [21] have compared mathematical models proposed by various researchers and it has been reported that the model proposed by Kumar and Tiwari [22] predicts yield which is in good agreement with the experimental results. As the model is based on linear regression and hence not bound by the Gr range. Inputs required in this model are experimental distillate output, the intensity of solar radiation, the temperature of the water, condensing cover and ambient air for calculating the values of C and n . Hence, in this manuscript, the model proposed by Kumar and Tiwari [22] has been used. The mathematical equations used in this model are as follows:

$$\dot{m} = 0.0163(P_w - P_g) \frac{k}{d} \frac{3,600}{L} C (\text{Gr} \cdot \text{Pr})^n \quad (7)$$

$$\ln\left(\frac{\dot{m}}{\Re}\right) = \ln(C) + n \cdot \ln(\text{Gr} \cdot \text{Pr}) \quad (8)$$

$$\text{where } \Re = 0.0163(P_w - P_g) \frac{k}{d} \frac{3,600}{L}.$$

Eq. (8) may be rewritten as:

$$y = a + n \cdot x \quad (9)$$

where $y = \ln\left(\frac{\dot{m}}{\Re}\right)$, $a = \ln(C)$ and $x = \ln(\text{Gr} \cdot \text{Pr})$.

The values of C and n from this model are as follows:

$$n = \frac{N(\sum xy) - (\sum x) \times (\sum y)}{N(\sum x^2) - (\sum x)^2} \quad (10)$$

$$C = \exp\left(\frac{(\sum y)}{N} - n \frac{(\sum x)}{N}\right) \quad (11)$$

After calculating $h_{c,w-g}$, $h_{e,w-g}$ can be calculated using the following relation:

$$h_{e,w-g} = 0.016273 \times h_{c,w-g} \times \frac{P_w - P_g}{T_w - T_g} \quad (12)$$

After calculating convective and evaporative heat transfer coefficients, theoretical distillate output can be evaluated by:

$$\dot{m}_{ew} = \frac{h_{e,w-g} \times A_g \times (T_w - T_g) \times 3,600}{L} \quad (13)$$

Radiative heat transfer coefficient from water to condensing glass cover surface can be written as [17]:

$$h_{r,w-g} = \epsilon_{\text{eff}} \times \sigma \times \left\{ (T_w + 273.15)^2 + (T_g + 273.15)^2 \right\} \times (T_w + T_g + 546.2) \quad (14)$$

where $\frac{1}{\epsilon_{\text{eff}}} = \frac{1}{\epsilon_w} + \frac{1}{\epsilon_g} - 1$.

Total internal heat transfer coefficient from water to condensing glass cover surface is calculated by adding convective, evaporative and radiative heat transfer coefficients as follows:

$$h_{t,w-g} = h_{c,w-g} + h_{e,w-g} + h_{r,w-g} \quad (15)$$

Total internal heat transfer coefficient from water to condensing glass cover surface one can get: $q_{t,w-g} = q_{c,w-g} + q_{e,w-g} + q_{r,w-g} = h_{t,w-g} \times (T_w - T_g)$.

Energy fraction of each mode of heat transfer, one can get [17]:

$$F_{e,w-g} = \frac{\dot{q}_{e,w-g}}{\dot{q}_{t,w-g}}; F_{c,w-g} = \frac{\dot{q}_{c,w-g}}{\dot{q}_{t,w-g}}; F_{r,w-g} = \frac{\dot{q}_{r,w-g}}{\dot{q}_{t,w-g}} \quad (16)$$

The hourly thermal efficiency of the solar still is defined as the ratio of thermal energy extracted to obtain an amount of distillate output in an hour to the total solar energy input during that hour. This can be calculated by the following equation [23]:

$$\eta = \frac{\dot{m}_{ew} \times L}{I(t) \times A_w \times 3600} \quad (17)$$

Exergy efficiency is defined as the ratio of exergy of evaporation to the exergy input [24]:

$$\eta_{Ex} = \frac{\dot{Ex}_e}{\dot{Ex}_i} \quad (18)$$

Exergy destruction for basin area, glass surface and water is calculated using the relation [16,23]:

$$\dot{Ex}_{d,b} = (\tau_g \tau_w \alpha_b \dot{Ex}_i) - (\dot{Ex}_w + \dot{Ex}_{\text{insu}}) \quad (19)$$

$$\dot{Ex}_{d,g} = (\alpha_g \dot{Ex}_i) + (\dot{Ex}_{\text{tr},w-g} - \dot{Ex}_{\text{tr},g-a}) \quad (20)$$

$$\dot{Ex}_{d,w} = (\tau_g \alpha_w \dot{Ex}_i) + (\dot{Ex}_w - \dot{Ex}_{\text{tr},w-g}) \quad (21)$$

Cost analysis of the solar still is performed using the following relations [16,25]:

Capital recovery factor:

$$\text{CRF} = \frac{i'(1+i')^{n'}}{(1+i')^{n'} - 1} \quad (22)$$

Sinking fund factor:

$$\text{SFF} = \frac{i'}{(1+i')^{n'} - 1} \quad (23)$$

Salvage value:

$$S' = \frac{1}{2} \times S \quad (24)$$

First annual cost:

$$\text{FAC} = (\text{CRF}) \times P' \quad (25)$$

Annual salvage value:

$$\text{ASV} = (\text{SFF}) \times S' \quad (26)$$

Annual maintenance cost (AMC):

$$\text{AMC} = 0.15 \times \text{FAC} \quad (27)$$

Total annual cost:

$$\text{TAC} = \text{FAC} + \text{AMC} - \text{ASV} \quad (28)$$

Cost per L:

$$\text{CPL} = \frac{\text{TAC}}{\text{AY}} \quad (29)$$

Cost payback calculations are done using a simple payback method with equal annual savings [25]. The payback period of the distiller unit can be calculated by dividing initial investment by annual operating cash (AOC) flow. AOC flow, AOC = cost of the product (as per prevailing market price) – AMC. Considering the sales price in Indian national rupee (INR) of distilled water as 20 INR/l.

$$\text{AOC} = \text{AY} \times 20 - \text{AMC} \quad (30)$$

Payback period:

$$\text{PB} = \frac{P'}{\text{AOC}} \quad (31)$$

4. Results and discussion

Variation of recorded incident solar radiation on east and west inclined cover surface as a function of time is illustrated in Fig. 5. The maximum incident solar radiation is measured as 1,175 and 1,150 W/m² on the east and west top covers of distiller units, at 11:00 and 14:00 h, respectively. The average incident solar radiation during the experimentation on a sunny day is 612.46 W/m². The slope of the curve is more on the east top cover than the west one till noon whereas, from noon till evening the slope is higher for west top cover than the east one, due to 15° cover inclination.

Variation in the ambient, and water and glass temperature in CDSSS and MDSSS as a function of time are shown in Fig. 6. The temperature of water and glass increases in both CDSSS and MDSSS from 6:00 to 13:00 h, then from 13:00 to 19:00 h it declines. The temperatures of water and the inner surface of condensing cover in MDSSS are higher than CDSSS. The reason for the higher water temperature in MDSSS may be because of a reduction in specific heat due to the application of the magnetic field, but the higher

temperature of the inner condensing surface is probably due to higher condensation rates than CDSSS. The ambient temperature increases from 6:00 to 12:00 h, remains steady from 12:00 to 13:00 h and then from 13:00 to 19:00 h it decreases. The difference between the temperatures of the water and the inner glass surface of, in CDSSS and MDSSS, first drops from 6:00 to 8:00 due to an increase of cover temperature at a higher rate, then it increases. This difference is maximum (5.15°C) at 14:00 h in CDSSS and in MDSSS it is maximum (6.55°C) at 13:00 h. Average water temperature, average condensing cover temperature and the average difference between water and condensing cover, of MDSSS, are respectively, 3.76%, 2.89%, and 14.16% higher than CDSSS.

Partial pressures of air vapor mixture is a function of temperature. Hence the partial pressures of water and condensing cover also rise and fall with temperatures. Based on temperatures measured, partial pressures are evaluated and their variations are illustrated with respect to the time in Fig. 7. The difference of partial pressure at the evaporating water surface and the condensing cover surface is responsible for convective and evaporative heat and mass transfer.

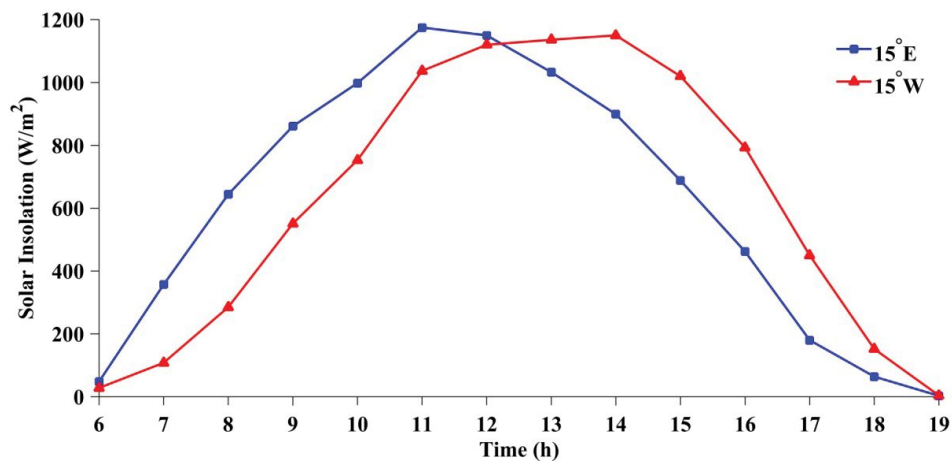


Fig. 5. Hourly variation of incident solar radiation with respect to time.

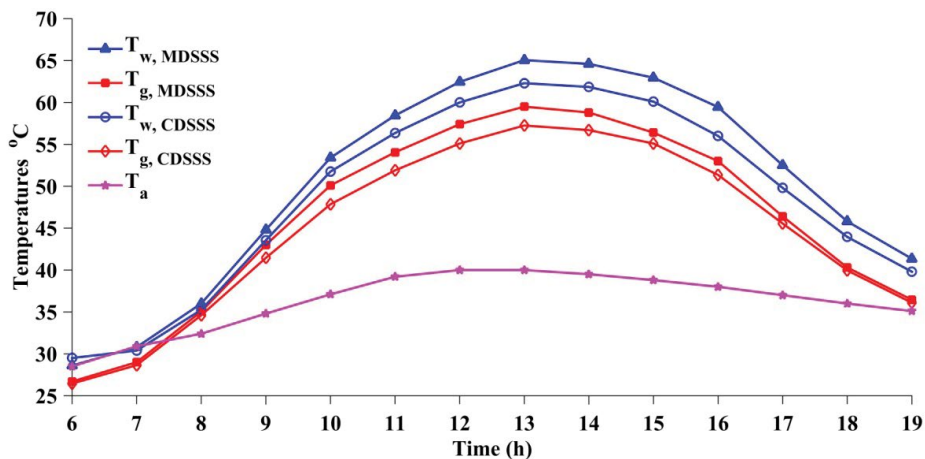


Fig. 6. Variation of temperatures in CDSSS and MDSSS.

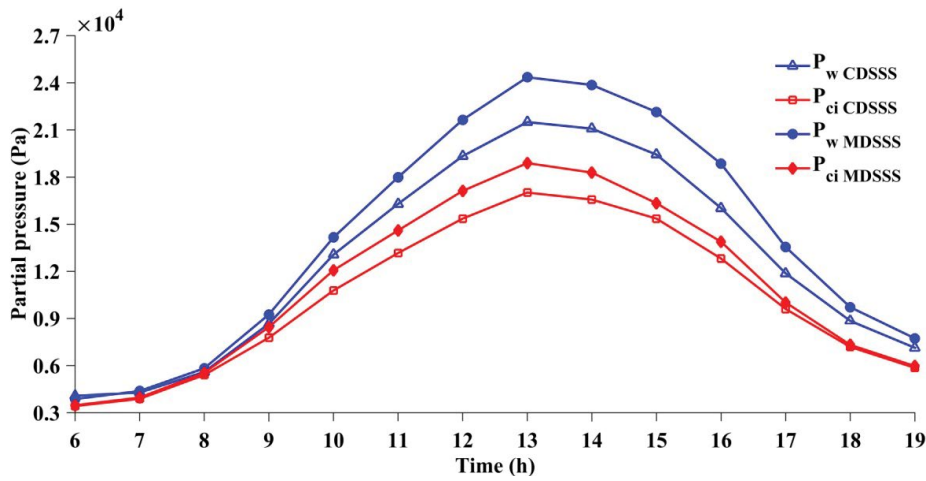


Fig. 7. Variation in partial pressure with respect to the time.

The difference in the partial pressure of water and the inner condensing cover is improved by 25.43% because of surface tension reduction due to the presence of a magnetic field.

Internal heat transfer in a solar still is governed by evaporative, convective and radiative heat transfer coefficients. These coefficients are evaluated on an hourly basis and shown in Fig. 8. The evaporative heat transfer coefficient remains almost constant from 6:00 to 8:00 h, it rises from 8:00 to 13:00 h, then falls from 13:00 to 19:00 h in both the stills. The convective heat transfer coefficient drops in both the stills from 6:00 to 8:00 h. In CDSSS it rises from 8:00 to 13:00 h whereas in MDSSS it rises from 8:00 to 15:00 h. Then it decreases in both the stills. The radiative heat transfer coefficient escalates in both the stills from 6:00 to 13:00 h, then decline from 13:00 to 19:00 h. In a solar still, the order of magnitudes of evaporative, radiative and convective heat transfer coefficient is decreasing one. As temperature hikes, evaporative heat transfer coefficients accelerate at a much higher rate in comparison to convective and radiative heat transfer coefficients. Hence the modification that enhances the evaporative heat transfer

coefficient is considered as a better option. The magnetization has enhanced the evaporative, convective and radiative heat transfer coefficients by 21.77%, 11.32%, and 1.53%, respectively.

The total heat transfer coefficient comprises evaporative, convective and radiative heat transfer coefficients. Fig. 9 illustrates the variation of total heat transfer coefficient with respect to time. It almost remains constant from 6:00 to 8:00 h, from 8:00 to 14:00 h it increases and then decreases from 14:00 to 19:00 h. At 14:00 h overall heat transfer coefficient of MDSSS reaches the highest value of 47.48 W/m² K, which is 19.2% greater than the CDSSS. The average overall heat transfer coefficient of MDSSS is 30.17 W/m² K, which is 16.26% higher in comparison with the CDSSS.

The variation in the rate of internal heat transfer of both the stills, from water to condensing glass cover, is represented in Fig. 10. From 6:00 to 8:00 h it decreases slightly in both the stills. Then from 8:00 to 15:00 h it accelerates with 78.9 W/h in MDSSS, which is 105% higher than that of CDSSS. After attaining its highest magnitude, its value falls in both the stills. The maximum and average heat transfer

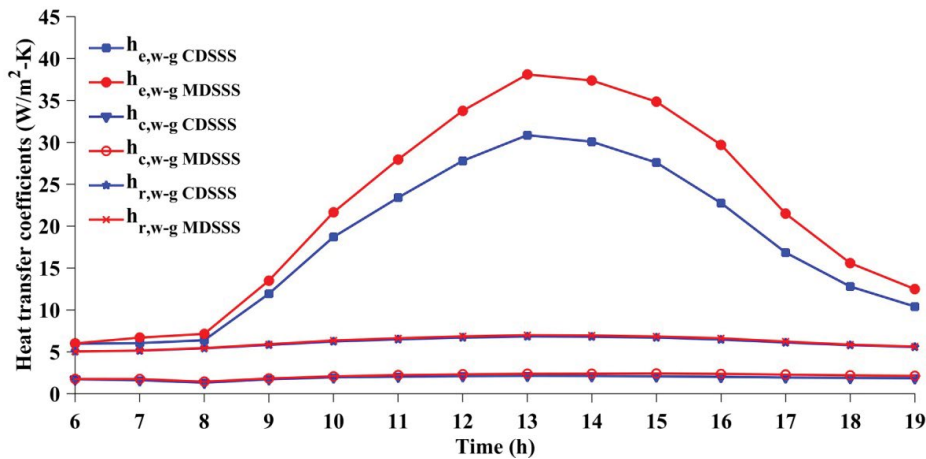


Fig. 8. Variation of evaporative, convective and radiative heat transfer coefficients with respect to the time.

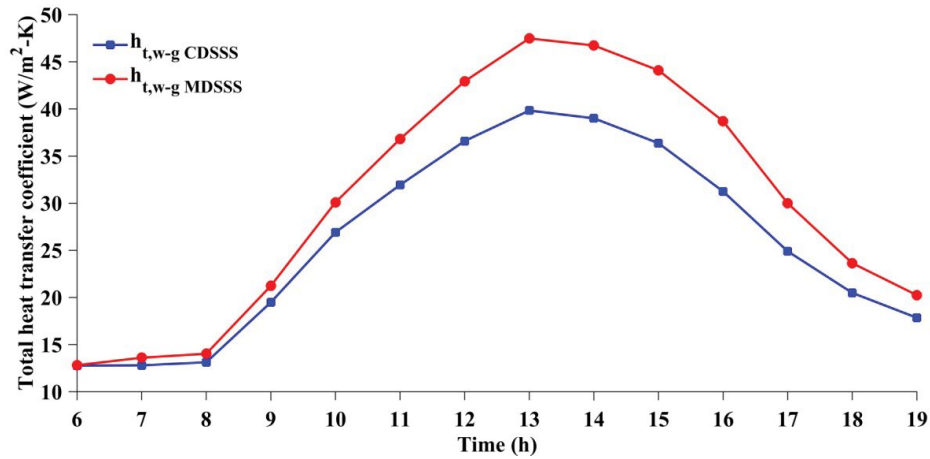


Fig. 9. Variation of total heat transfer coefficient with respect to the time.

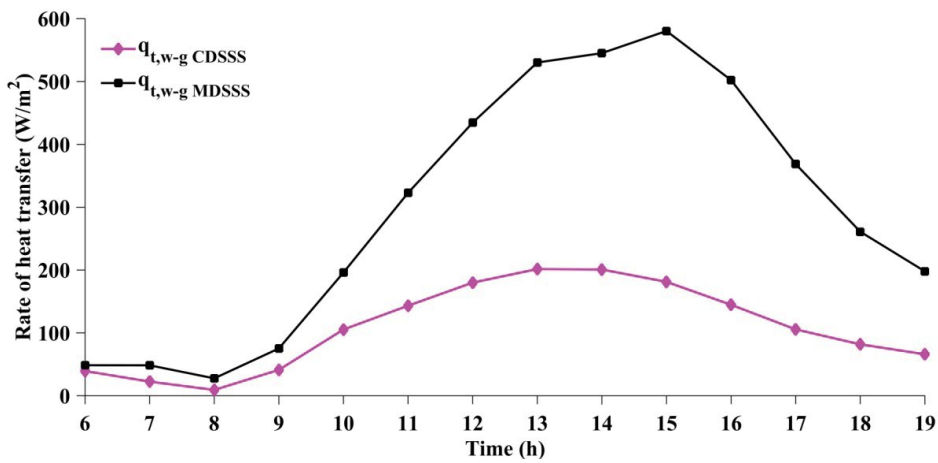


Fig. 10. Variation in heat transfer rate with respect to the time.

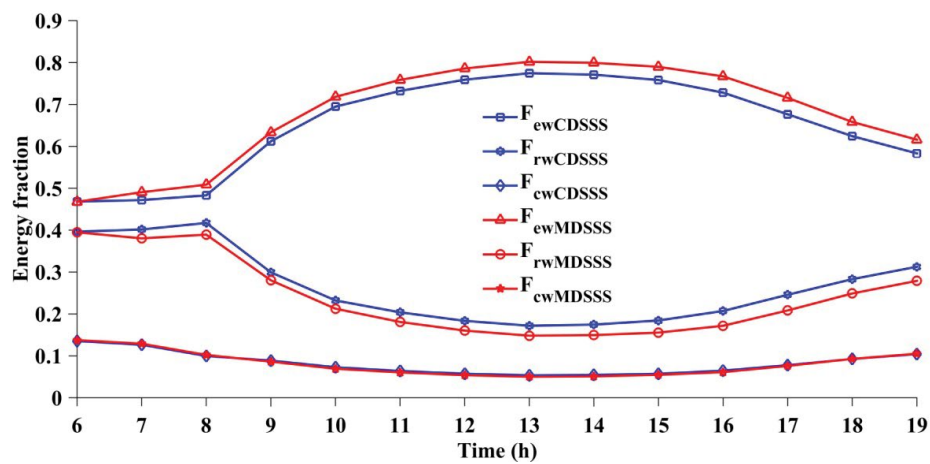


Fig. 11. Variation of energy fraction with respect to the time.

rate of MDSSS is 580.38 and 295.62 W/m², which are respectively 187.94% and 171.83% higher than CDSSS. This high value of overall heat transfer in MDSSS are owing to the fact that there has been a substantive reduction in the surface

tension of water due to its magnetization on one hand and reduction in the thickness of water above the GI sheet.

The contribution of various modes of heat transfer is computed for both the solar stills as energy fraction

and is shown in Fig. 11. The evaporative energy fraction increases with an increase in temperature whereas convective and radiative energy fractions decrease, as the temperatures increase. When the temperatures drop, their behavior reverses. In both the stills, the evaporative energy fraction escalates slowly from 6:00 to 8:00 h then accelerates from 8:00 to 13:00 h, attains top at 13:00 h and then reduces. The maximum and average evaporative fraction of MDSSS are 0.8 and 0.68 respectively which are 3.51% and 4.08% above that of CDSSS. In both the stills, the convective energy fraction initially rises a little from 6:00 to 8:00 h, then decelerates rapidly, touches its lowest value at 13:00 h and again raises from 13:00 to 19:00 h. Throughout the experiment, the radiative energy fraction of CDSSS takes over that of MDSSS. The maximum and average energy fraction of MDSSS is 5.34% and 9.52% below the CDSSS, and is 0.39 and 0.24, respectively. In both the stills the convective energy fraction reduces from 6:00 to 13:00 h then increases from 13:00 to 19:00 h. The convective energy fraction of MDSSS is 1.39% lower than CDSSS.

Fig. 12 illustrates the variation of experimental and theoretical instantaneous thermal efficiencies of MDSSS and CDSSS. The magnitudes of efficiencies from 7:00 to

16:00 h are shown. In both the stills, there is good agreement between theoretical and experimental results. In both, the stills experimental and theoretical efficiencies decrease from 7:00 to 8:00 h then rise from 8:00 to 16:00 h. In CDSSS, experimental efficiency is 14.45% higher than theoretical efficiency whereas in MDSSS experimental efficiency is 11.07% higher than theoretical efficiency. The experimental efficiency of MDSSS leads to CDSSS by 22.64%.

Exergy efficiency is the ratio of exergy output associated with the distillate output of a solar still to the exergy input of radiation. Hourly evaluation of the exergy of CDSSS and MDSSS is represented in Fig. 13. The exergy efficiency of CDSSS decreases from 6:00 to 7:00 h, remains very low from 7:00 to 8:00 h and then increases till 18:00 h. In MDSSS the exergy efficiency remains low from 6:00 to 8:00 h then increases. The exergy efficiency of MDSSS is 57.58% higher than CDSSS.

Exergy destruction in water, basin line and glass are evaluated for both the stills and are shown in Fig. 14. It shows that the maximum hourly exergy destruction in glass, water, and basin liner of MDSSS reaches up to 55.75, 35.42 and 596.83 W, respectively which are 4.91% higher, 11.63% and 10.82% lower than CDSSS, respectively. In

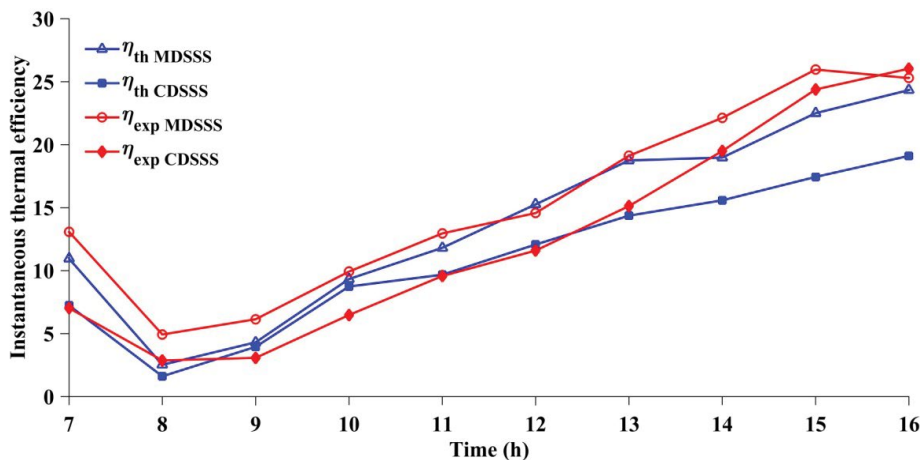


Fig. 12. Variation of theoretical and experimental efficiency in CDSSS and MDSSS with respect to the time.

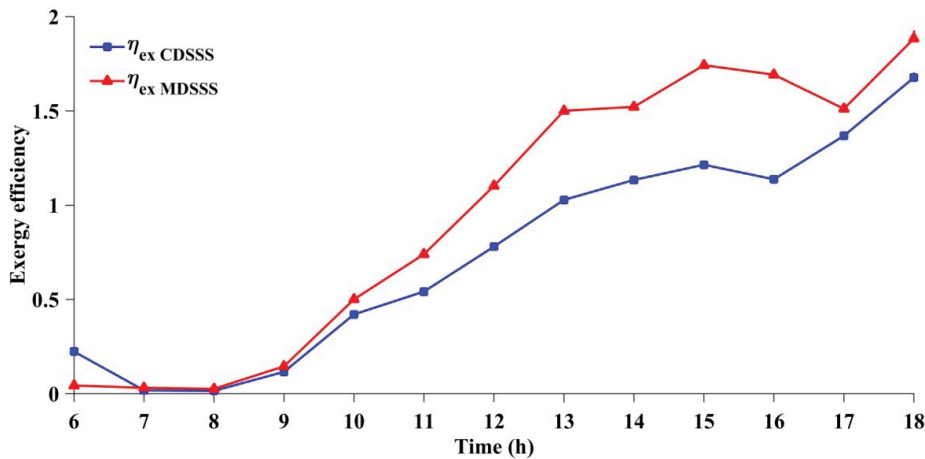


Fig. 13. Variation of exergy efficiency of CDSSS and MDSSS with respect to the time.

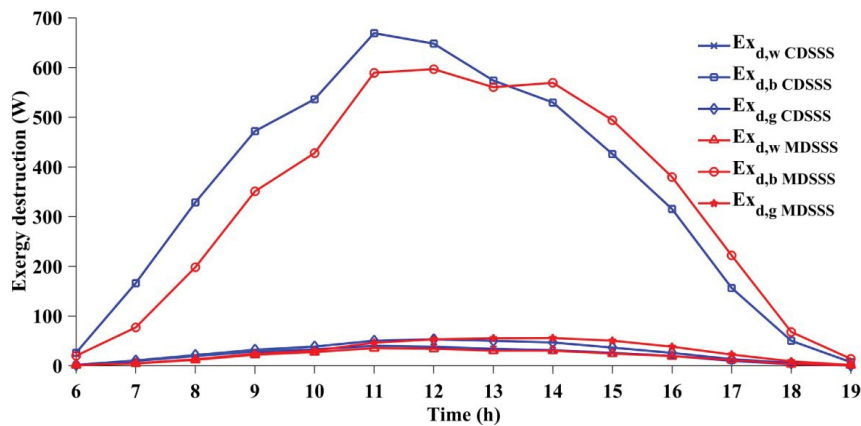


Fig. 14. Variation of exergy destruction in CDSSS and MDSSS with respect to the time.

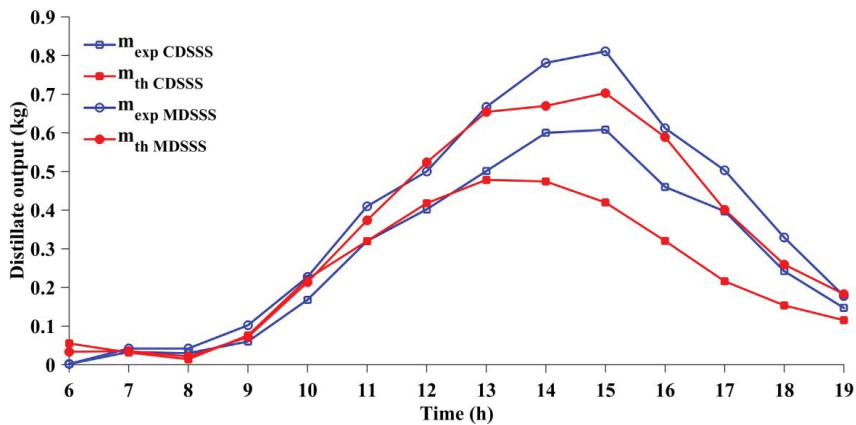


Fig. 15. Variation of experimental and theoretical distillate output in CDSSS and MDSSS with respect to the time.

MDSSS the average exergy destruction in glass, water and basin liner has been 28.96, 18.38 and 326.24 W, respectively which are 4.89% higher, 12.71% and 6.9% lower than CDSSS. Here, it can be noticed that exergy destruction from water, glass and basin liner very much depends upon the solar insolation.

The variation in theoretical and experimental distillate yield obtained from CDSSS and MDSSS as a function of time is shown in Fig. 15. The maximum hourly distillate output of MDSSS is 0.81 kg which is 33.39% above that of CDSSS. The cumulative distillate output of MDSSS during sunshine hours is 5.206 kg which exceeds CDSSS by 31.13%. The cumulative output of MDSSS, for 24 h (adding the output of nocturnal hours) is 5.901 kg which is 29.59% above CDSSS. The average hourly theoretical distillate output of CDSSS and MDSSS are 0.37 and 0.34 kg, respectively which are 16.51% and 9.12% less than their experimental values. However, the hourly experimental distillate outputs exhibit good agreement with their theoretical values.

The cost of installation and salvage value of CDSSS and MDSSS are tabulated in Tables 1 and 2, respectively. Calculation of various cost components (viz. cost of production, payback period) are tabulated in Table 3.

Table 1
Cost installation of CDSSS

Material	Cost (INR)	Cost of salvageable item (INR)
Fibre reinforced plastic still	6,000	1,000
Glass	1,000	–
Putty	500	–
Tubing	50	–
	$P'_{CDSSS} = 7,550$ INR	$S_{CDSSS} = 1,000$ INR

5. Conclusions

On the basis of the experimental and theoretical results of single basin double slope passive solar still, with and without augmentation effect of permanent ferrite ring magnets following conclusions are drawn:

- Distillate output of MDSSS during sunshine hours (6:00–19:00 h) and in 24 h is 5.206 and 5.901 kg which is 31.13% and 29.59% higher than CDSSS respectively (Fig. 15).

Table 2
Cost of installation of MDSSS

Material	Cost (INR)	Cost of salvageable item (INR)
Fibre reinforced plastic still	6,000	1,000
Glass	1,000	–
Putty	500	–
GI sheet	300	100
Ferrite ring magnets	3,000	500
Tubing	50	–
	$P'_{MDSSS} = 10,850$ INR	$S_{MDSSS} = 1,600$ INR

Table 3
Cost calculations of CDSSS and MDSSS

Cost component	CDSSS	MDSSS
Annual interest rate, i'	12%	12%
Life of still in years, n' (y)	15 y	15 y
Capital recovery factor, CRF	0.1468	0.1468
Sinking fund factor, SFF	0.0268	0.0268
First annual cost, FAC (INR)	1,108.34	1,592.78
S' (INR)	500.00	800.00
Annual salvage value, ASV (INR)	13.40	21.44
Annual maintenance cost, AMC (INR)	166.25	238.92
Total annual cost, TAC (INR)	1,261.19	1,810.26
Annual yield, AY (l)	1,661.48	2,153.13
Cost per L, CPL (INR/l)	0.76	0.84
Annual operating cash, AOC (INR)	33,063.35	42,823.68
Payback period, PB (y)	0.22	0.25

- Cumulative theoretical distillate output of MDSSS and CDSSS is 9.12% and 16.51% less, respectively than their experimental values (Fig. 15).
- Magnetic field has improved the partial pressure difference between water and inner condensing cover by 25.43% (Fig. 7).
- Evaporative and total heat transfer coefficients have enhanced by 21.77% and 16.26% respectively, due to augmentation (Figs. 8 and 9).
- Rate of heat transfer of MDSSS is enhanced by 171.83% due to the magnetization of water (Fig. 10).
- Experimental efficiency of MDSSS is 22.64% higher than CDSSS (Fig. 12).
- Exergy efficiency of MDSSS has boosted by 57.58% in comparison to CDSSS (Fig. 13).
- Maximum exergy destruction occurs in the basin followed by glass and water (Fig. 14).
- Payback periods of both the stills are less than 3 months.

It may be concluded that the magnetization has an edge over conventional still to improve its distillate yield.

Symbols

- A – Area, m²
- AY – Annual yield, l

- C – Constant
- c – Specific heat, J/kg K
- d – Characteristic length of the solar still
- \dot{E}_x – Exergy, W
- F – Energy fraction
- g – Acceleration due to gravity, m/s²
- Gr – Grashof number
- h – Heat transfer coefficient, W/m² K
- i' – Annual interest rate, %
- $I(t)$ – Incident solar radiation on inclined glass cover, W/m²
- k – Thermal conductivity of humid air, W/m K
- L – Latent heat of vaporization, J/kg
- \dot{m} – Mass of distillate output, kg/m² h
- Nu – Nusselt number
- n – Constant
- n' – Life of still in years
- P – Saturated vapor pressure, Pa
- P' – Initial investment in INR
- PB – Payback period, years
- Pr – Prandtl number
- \dot{q} – Rate of heat transfer, W/m²
- \mathfrak{R} – Universal gas constant, $\mathfrak{R} = 8.314$ k J/k mol K
- Ra – Rayleigh number
- S – System salvage value in INR
- T – Temperature, °C

Subscripts

- a – Ambient
- b – Basin
- c – Convective
- d – Destruction
- e – Evaporative
- eff – Effective
- ex – Exergy
- exp – Experimental
- ew – Distillate water
- g – Glass condensing cover
- i – Insulation
- l – Loss
- p – Pressure
- r – Radiative
- t – Total
- th – Theoretical
- tr – Transfer
- w – Water

Greek

α	—	Absorptivity
β	—	Volume expansivity, K^{-1}
$\Delta T'$	—	Effective temperature difference, $^{\circ}C$
η	—	Efficiency

References

- [1] T.V. Arjunan, H.Ş. Aybar, N. Nedunchezian, Status of solar desalination in India, *Renewable Sustainable Energy Rev.*, 13 (2009) 2408–2418.
- [2] T. Arunkumar, K. Raj, D. Dsilva Winfred Rufuss, D. Denkenberger, G. Tingting, L. Xuan, R. Velraj, A review of efficient high productivity solar stills, *Renewable Sustainable Energy Rev.*, 101 (2019) 197–220.
- [3] S.J.P. Gnanaraj, V. Velmurugan, An experimental study on the efficacy of modifications in enhancing the performance of single basin double slope solar still, *Desalination*, 467 (2019) 12–28.
- [4] M. Dubey, D.R. Mishra, Experimental and theoretical evaluation of double slope single basin solar stills: study of heat and mass transfer, *FME Trans.*, 47 (2019) 101–110.
- [5] L. Holysz, A. Szczes, E. Chibowski, Effects of a static magnetic field on water and electrolyte solutions, *J. Colloid Interface Sci.*, 316 (2007) 996–1002.
- [6] Y.-Z. Guo, D.-C. Yin, H.-L. Cao, J.-Y. Shi, C.-Y. Zhang, Y.-M. Liu, H.-H. Huang, Y. Liu, Y. Wang, W.-H. Guo, A.-R. Qian, P. Shang, Evaporation rate of water as a function of a magnetic field and field gradient, *Int. J. Mol. Sci.*, 13 (2012) 16916–16928.
- [7] Y.K. Wang, H.N. Wei, Z.W. Li, Effect of magnetic field on the physical properties of water, *Results Phys.*, 8 (2018) 262–267.
- [8] H.B. Amor, A. Elaoud, N.B. Salah, K. Elmoueddeb, Effect of magnetic treatment on surface tension and water evaporation, *Int. J. Adv. Ind. Eng.*, 5 (2017) 119–124.
- [9] R. Cai, H.W. Yang, J.S. He, W.P. Zhu, The effects of magnetic fields on water molecular hydrogen bonds, *J. Mol. Struct.*, 938 (2009) 15–19.
- [10] F.L. Rashid, N.M. Hassan, A.M. Jafar, A. Hashim, Increasing water evaporation rate by magnetic field, *Int. Sci. Invest. J.*, 2 (2013) 61–68.
- [11] K.-T. Chang, C.-I. Weng, The effect of an external magnetic field on the structure of liquid water using molecular dynamics simulation, *J. Appl. Phys.*, 100 (2006) 1–6.
- [12] J. Nakagawa, N. Hirota, K. Kitazawa, M. Shoda, Magnetic field enhancement of water vaporization, *J. Appl. Phys.*, 86 (1999) 2923–2925.
- [13] A. Seyfi, R. Afzalzadeh, A. Hajnorouzi, Increase in water evaporation rate with increase in static magnetic field perpendicular to water-air interface, *Chem. Eng. Process. Process Intensif.*, 120 (2017) 195–200.
- [14] A. Szcześ, E. Chibowski, L. Holysz, P. Rafalski, Effects of static magnetic field on water at kinetic condition, *Chem. Eng. Process. Process Intensif.*, 50 (2011) 124–127.
- [15] N.S. Zaidi, J. Sohaili, K. Muda, M. Sillanpää, Magnetic field application and its potential in water and wastewater treatment systems, *Sep. Purif. Rev.*, 43 (2014) 206–240.
- [16] P. Dumka, Y. Kushwah, A. Sharma, D.R. Mishra, Comparative analysis and experimental evaluation of single slope solar still augmented with permanent magnets and conventional solar still, *Desalination*, 459 (2019) 34–45.
- [17] G.N. Tiwari, A.K. Tiwari, *Solar Distillation Practice for Water Desalination Systems*, Anamaya, New Delhi, 2008.
- [18] S. Toyama, T. Aragak, H.M. Salah, K. Murase, M. Sando, Simulation of a multieffect solar still and the static characteristics, *J. Chem. Eng. Jpn.*, 20 (1987) 473–478.
- [19] J.A. Clark, The steady-state performance of a solar still, *Sol. Energy*, 44 (1990) 43–49.
- [20] R.V. Dunkle, *Solar Water Distillation: The Roof Type Still and a Multiple Effect Diffusion Still*, International Heat Transfer Conference, Boulder, Colo. and Westminster, London, England, 1961–1962, 895–902p.
- [21] P. Dumka, D.R. Mishra, Energy and exergy analysis of conventional and modified solar still integrated with sand bed earth: study of heat and mass transfer, *Desalination*, 437 (2018) 15–25.
- [22] S. Kumar, G.N. Tiwari, Estimation of convective mass transfer in solar distillation systems, *Sol. Energy*, 57 (1996) 459–464.
- [23] P. Dumka, D.R. Mishra, Experimental investigation of modified single slope solar still integrated with earth (I) & (II): energy and exergy analysis, *Energy*, 160 (2018) 1144–1157.
- [24] R. Petela, Exergy of undiluted thermal radiation, *Sol. Energy*, 74 (2003) 469–488.
- [25] K. Mukherjee, G.N. Tiwari, Economic analyses of various designs of conventional solar stills, *Energy Convers. Manage.*, 26 (1986) 155–157.